

Blueshifts in the Lemaître – Tolman models

Andrzej Krasiński

*N. Copernicus Astronomical Centre,
Polish Academy of Sciences,
Bartycka 18, 00 716 Warszawa, Poland**

(Dated:)

In the Lemaître – Tolman (L–T) models that have nonconstant bang-time function $t_B(r)$, light emitted close to those points of the Big Bang where $dt_B/dr \neq 0$ is blueshifted at the receiver position. The blueshifted rays are expected to perturb the temperature of the cosmic microwave background radiation along the lines of sight of the present central observer. It is shown here that, in a general L–T model, the $t_B(r)$ can be chosen so that the blueshift-generating region is hidden before the recombination time, where the L–T model does not apply. The rest of the paper is devoted to investigating blueshifts in one specific L–T model, called L–T(t_B) – the one that duplicates the luminosity distance vs. redshift relation of the Λ CDM model using nonconstant $t_B(r)$ alone. The location of the blueshift-generating region in the L–T(t_B) spacetime is determined. Profiles of redshift/blueshift along several rays intersecting the past light cone of the present central observer are calculated. The L–T(t_B) model matched to Friedmann is considered, and profiles of redshift/blueshift in such a composite model are calculated. The requirement of invisibility of blueshifts makes the L–T(t_B) model astrophysically unacceptable if it should apply back to the recombination time, but does not “rule out” a general L–T model – it only puts limits on dt_B/dr .

PACS numbers:

Keywords:

I. MOTIVATION AND BACKGROUND

It was argued [1] that the Lemaître [2] – Tolman [3] (L–T) models with nonconstant bang-time function $t_B(r)$ are “ruled out” because of spectral distortions of light received by the present central observer that such t_B would cause. The spectral distortions are expected to arise when blueshifted rays emitted close to those points of the Big Bang (BB) where $dt_B/dr \neq 0$ intersect the past light cone of the present central observer (PCPO). Investigating the blueshifts and possible spectral distortions caused by them is a valid research problem. However, although Ref. [1] arose out of criticism of the so-called “void models of acceleration”, the particular L–T model considered there did not correspond to any real situation in the Universe (see Appendix A).¹

In the present paper, the blueshifts are investigated in a general L–T model, and in the model that was derived in Ref. [4] by the method introduced in Ref. [5]. In the latter, called here the L–T(t_B) model, the accelerated expansion of the Universe is simulated using a suitably (numerically) constructed nonconstant $t_B(r)$, with the other L–T free function, $E(r)$, having the same form as in the Friedmann model: $E = -kr^2/2$, where k is a constant. The equations that ensure the simulation imply

a unique value of $k < 0$, see Sec. II.

In an L–T model with nonconstant t_B , blueshifts are generated only close to the BB [6, 7]. Observers who carry out their observations far from the BB see light from nearby objects being redshifted. However, light rays emitted from the BB at those points, where $dt_B/dr \neq 0$, behave in a peculiar way. When a radially directed ray of this class is followed back in time beginning at a late-epoch observer, the redshift along it at first increases from zero, but reaches a maximum, then decreases to become negative (i.e. to turn to blueshift) at some point, to finally become -1 at the contact with the BB. The value $z = -1$ is referred to as *infinite blueshift* [6, 7], see Sec. II. The locus, where the redshift along radial rays acquires a maximum, will be termed maximum-redshift hypersurface (MRH). The locus, where the observed redshift along these rays turns to blueshift, will be termed zero-redshift hypersurface (ZRH).

To display blueshift to the observer, a ray must build up a sufficiently large blueshift *before* it intersects ZRH, in order to offset the redshift accumulated in the later part of the path. Thus, along any ray, the MRH is later than the ZRH. Along radial rays, the MRH is observer-independent (see Sec. IV).

The ZRH is defined only with respect to a given family of observers, and is different for each family. If ZRH is closer to the BB than the last-scattering hypersurface, then the blueshifts are hidden in the pre-recombination era, where the zero-pressure L–T models do not apply. This is why it is important to locate the ZRH in spacetime, relative to those events, where spectral distortions would be observable; namely, events along the ray emitted from the last-scattering hypersurface that reaches the central observer at present.

*Electronic address: akr@camk.edu.pl

¹ The author of Ref. [1] claimed that he ruled out L–T models “with significant decaying mode contribution today”. But the further comments leave the reader with the impression that the whole L–T class was killed, even though the assumptions actually made ($E = 0$ and a specific $t_B(r)$ profile) were strongly restricting.

An L–T metric is never meant to be a global model of the whole Universe. Any given L–T metric is always meant to model a limited part of our spacetime. It should be matched to a background metric modelling the rest of the Universe, for example a Friedmann metric. In the case of the L–T models that simulate accelerated expansion, it makes sense to apply them only out to such distances, at which the type Ia supernovae (SNIa) are observed. At present, the largest redshift observed for a type Ia supernova is $z \approx 1.9$ [8]; for the supernovae included in the two original projects [9, 10], the largest z was 0.83 [10].

The plan of the paper is as follows. Section II recalls basic properties of the L–T models. In Sec. III, it is shown that in a general L–T model, $|dt_B/dr|$ can always be made sufficiently small to hide the blueshifts in the pre-recombination epoch, where the assumption of zero pressure is not realistic, so the L–T model cannot apply.

The rest of the paper is devoted to the L–T(t_B) model only. In Sec. IV, the MRH of the central observer is determined and displayed. In Sec. V, the profiles of redshift are calculated along a few characteristic radial rays intersecting the PCPO. In Sec. VI, the L–T(t_B) model is matched to the Friedmann model across the matter world-tube that intersects the PCPO at $z = 0.83$, and profiles of redshift/blueshift along a few characteristic light cones are displayed. Section VII contains conclusions and a summary. In Appendix A, deficiencies of the model used in Ref. [1] are presented.

II. THE LEMAÎTRE – TOLMAN MODELS

This is a summary of basic facts about the L–T models. For extended expositions see Refs. [11, 12].

A. General facts

The numbering of the coordinates will be $(x^0, x^1, x^2, x^3) = (t, r, \vartheta, \varphi)$ and the signature will be $(+---)$. The metric of the model is

$$ds^2 = dt^2 - \frac{R_{,r}^2}{1 + 2E(r)} dr^2 - R^2(t, r)(d\vartheta^2 + \sin^2 \vartheta d\varphi^2), \quad (2.1)$$

where $E(r)$ is an arbitrary function. The source in the Einstein equations is dust, i.e. a pressureless fluid. The (geodesic) velocity field of the dust is

$$u^\alpha = \delta^\alpha_0. \quad (2.2)$$

The function $R(t, r)$ is determined by

$$R_{,t}^2 = 2E(r) + 2M(r)/R, \quad (2.3)$$

$M(r)$ being another arbitrary function; we neglect the cosmological constant. Throughout this paper only expanding models ($R_{,t} > 0$) will be considered. The solutions of (2.3) may be written as follows:

When $E > 0$:

$$\begin{aligned} R(t, r) &= \frac{M}{2E}(\cosh \eta - 1), \\ \sinh \eta - \eta &= \frac{(2E)^{3/2}}{M} [t - t_B(r)]; \end{aligned} \quad (2.4)$$

When $E = 0$:

$$R(t, r) = \left\{ \frac{9}{2} M(r) [t - t_B(r)]^2 \right\}^{1/3}; \quad (2.5)$$

When $E(r) < 0$:

$$\begin{aligned} R(t, r) &= -\frac{M}{2E}(1 - \cos \eta), \\ \eta - \sin \eta &= \frac{(-2E)^{3/2}}{M} [t - t_B(r)]; \end{aligned} \quad (2.6)$$

where $t_B(r)$ is one more arbitrary function called the bang time. The Big Bang occurs at $t = t_B(r)$.

The mass density is

$$\kappa \rho = \frac{2M_{,r}}{R^2 R_{,r}}, \quad \kappa \stackrel{\text{def}}{=} \frac{8\pi G}{c^2}. \quad (2.7)$$

Equations (2.1) – (2.7) are covariant with the transformations $r \rightarrow r' = f(r)$, which may be used to give one of the functions (M, E, t_B) a handpicked form, in the range where it is monotonic. In this paper, $M_{,r} > 0$ is assumed, and the following choice of r is made:

$$M = M_0 r^3, \quad (2.8)$$

where $M_0 > 0$ is an arbitrary constant. The transformations $r = Cr'$, with $C = \text{constant}$, are still allowed, and they redefine M_0 by $M_0 = M'_0/C^3$. So, we can assume $M_0 = 1$. Note that M_0 has the dimension of length and represents mass, so the choice of its value amounts to choosing a unit of mass – see Sec. II C.

A radial null geodesic is determined by the equation

$$\frac{dt}{dr} = \pm \frac{R_{,r}}{\sqrt{1 + 2E(r)}}, \quad (2.9)$$

where “+” applies to future outward-directed and past inward-directed geodesics, and “–” to the remaining ones. The solution of (2.9) is denoted $t = t_{\text{ng}}(r)$. The redshift $z(r)$ along $t_{\text{ng}}(r)$ is given by [13], [12]

$$\frac{1}{1+z} \frac{dz}{dr} = \left[\frac{R_{,tr}}{\sqrt{1 + 2E}} \right]_{\text{ng}}. \quad (2.10)$$

At the contact with the BB, null geodesics displayed in the comoving coordinates have horizontal tangents at those points, where $dt_B/dr = 0$, and have vertical tangents elsewhere. In the first case, $z \rightarrow \infty$ at the BB; in the second case, $z = -1$ at the BB, which is referred to as *infinite blueshift* [6, 7]. Indeed, $z < 0$ means that (frequency observed) $>$ (frequency at emission), so (frequency observed) $\rightarrow \infty$ when $z \rightarrow -1$ and the frequency

emitted is finite. However, it should be noted that a vertical tangent to a light ray at the BB, in comoving coordinates, means that matter particles are ejected from the BB with the velocity of light, i.e., a comoving observer at the BB would see zero frequency of the emitted light. So, some interpretation work is required to decide what an infinite blueshift actually means: magnifying a finite frequency to an infinitely hard blow at the observer, or shifting an unobservably soft radiation to the visible range. In all the Friedmann models (which are subcases of L–T), since t_B is constant, z is infinite at the BB.

In a general L–T model we have ([12], eqs. (18.104) and (18.112)):

$$R_{,r} = \left(\frac{M_{,r}}{M} - \frac{E_{,r}}{E} \right) R + \left[\left(\frac{3}{2} \frac{E_{,r}}{E} - \frac{M_{,r}}{M} \right) (t - t_B) - t_{B,r} \right] R_{,t} \quad (2.11)$$

when $E \neq 0$, and

$$R_{,r} = \frac{M_{,r}}{3M} R - \sqrt{\frac{2M}{R}} t_{B,r} \quad (2.12)$$

when $E = 0$.

Given a past-directed $t_{\text{ng}}(r)$ and $z(r)$, the luminosity distance $D_L(z)$ of a light source from the central observer is [14, 15]

$$D_L(z) = (1+z)^2 R(t_{\text{ng}}(r), r). \quad (2.13)$$

The model of Refs. [5] and [4], further investigated here, was constructed so that $D_L(z)$, calculated along the PCPO, is the same as in the Λ CDM model:

$$D_L(z) = \frac{1+z}{H_0} \int_0^z \frac{dz'}{\sqrt{\Omega_m(1+z')^3 + \Omega_\Lambda}}, \quad (2.14)$$

where H_0 is related to the Hubble ‘‘constant’’ \mathcal{H}_0 by $H_0 = \mathcal{H}_0/c$, and $(\Omega_m, \Omega_\Lambda) = (0.32, 0.68)$ are parameters defined by observations [16]; see Sec. II C.

Note that the duplication of $D_L(z)$ occurs only along a single light cone. Observations that are sensitive to the dynamics of the model, for example redshift drift [17], could distinguish between the Λ CDM and L–T models having the same $D_L(z)$ at present.

The $R_{\text{ng}}(r) \stackrel{\text{def}}{=} R(t_{\text{ng}}(r), r)$ in (2.13) is the angular diameter distance, and it is not an increasing function of r . At the intersection with the hypersurface $t(r)$, implicitly determined by the equation [18]

$$R = 2M, \quad (2.15)$$

the function $R_{\text{ng}}(r)$ acquires a maximum, and becomes decreasing for greater r . The hypersurface determined by (2.15) is called *apparent horizon* (AH). It is a difficult obstacle to numerical calculations because several quantities become 0/0 there, see Refs. [4, 19] and further references cited in them. Traces of those difficulties will

appear here in a few graphs as numerical instabilities. The values of r and z at the intersection of the PCPO with the AH in the L–T(t_B) model are [4]

$$\begin{pmatrix} r \\ z \end{pmatrix}_{\text{AH}} = \begin{pmatrix} 0.3105427968086945 \\ 1.582430687623614 \end{pmatrix}. \quad (2.16)$$

For technical reasons, the $t(r)$ and $z(r)$ curves crossing the point $r = r_{\text{AH}}$ were calculated separately in the ranges $r < r_{\text{AH}}$ and $r > r_{\text{AH}}$, as explained in Refs. [4] and [19]. Therefore, they are differently coloured in each of these ranges.

B. The L–T model with $2E = -kr^2$ that obeys (2.14)

This is the L–T(t_B) model. In it we have [4]

$$2E = -kr^2, \quad (2.17)$$

where $k < 0$ is a constant. This E is the same as in the $k < 0$ Friedmann model. Numerical fitting of the solution of (2.10) to the values of (r, z) at $(0, 0)$ and at the AH determined the value of k [4],

$$k = -4.7410812. \quad (2.18)$$

From (2.9) and (2.17) we have on a light cone

$$\frac{dt}{dr} = \pm \frac{R_{,r}}{\sqrt{1 - kr^2}}. \quad (2.19)$$

Using (2.8) and (2.17) we get from (2.11)

$$R_{,r} = \frac{R}{r} - rt_{B,r} \sqrt{\frac{2M_0 r}{R} - k}. \quad (2.20)$$

With (2.17), eqs. (2.4) become

$$\cosh \eta = 1 - \frac{kR}{M_0 r}, \quad (2.21)$$

$$t - t_B = \frac{M_0}{(-k)^{3/2}} (\sinh \eta - \eta). \quad (2.22)$$

Using (2.17) and (2.20) – (2.22), the set of equations $\{(2.19), (2.22), (2.10)\}$ was numerically solved in Ref. [4] for $t(r)$, $t_B(r)$ and $z(r)$ along the PCPO. The tables representing those solutions will be used here.

The L–T(t_B) model is determined around the center of symmetry up to those worldlines of dust that leave the BB at its contact with the PCPO. Extensions beyond the world-tube composed of those worldlines are possible, but are not determined by (2.13) – (2.14) and are not considered here. This model need not be used in this full range. A subset can be cut out of it and matched to a background model along a narrower world-tube.

C. The numerical units

The following values are assumed here:

$$(\Omega_m, \Omega_\Lambda, H_0, M_0) = (0.32, 0.68, 6.71, 1) \quad (2.23)$$

the first two after Ref. [16]. The H_0 is related to the Hubble constant \mathcal{H}_0 [16] by

$$\mathcal{H}_0 = cH_0 = 67.1 \text{ km}/(\text{s} \times \text{Mpc}), \quad (2.24)$$

so H_0 is measured in 1/Mpc. Consequently, choosing a value for H_0 amounts to defining a numerical length unit (NLU). Our time coordinate is $t = c\tau$, where τ is measured in time units, so t is measured in length units. So it is natural to take the NLU also as the numerical time unit (NTU). Taking for the conversion factors [20]

$$\begin{aligned} 1 \text{ pc} &= 3.086 \times 10^{13} \text{ km}, \\ 1 \text{ y} &= 3.156 \times 10^7 \text{ s}, \end{aligned} \quad (2.25)$$

the following relations result:

$$\begin{aligned} 1 \text{ NTU} &= 1 \text{ NLU} = 3 \times 10^4 \text{ Mpc} \\ &= 9.26 \times 10^{23} \text{ km} = 9.8 \times 10^{10} \text{ y}. \end{aligned} \quad (2.26)$$

The age of the Universe inferred from observations is [16]

$$T = 13.819 \times 10^9 \text{ y} = 0.141 \text{ NTU}. \quad (2.27)$$

As already mentioned below (2.8), M_0 represents mass, but has the dimension of length ($M_0 = Gm_0/c^2$, where m_0 is measured in mass units). The choice $M_0 = 1$ NLU made in (2.23) implies the mass unit $M_0c^2/G \approx 10^{54}$ kg, but it will not appear in any other way than via M_0 .

III. THE MAXIMUM-REDSHIFT HYPERSURFACE IN A GENERAL L–T MODEL

Consider a radial light ray $t_{\text{ng}}(r)$ reaching a comoving observer at a sufficiently late time (below, it will become clear what “sufficiently late” means). When we follow that ray back in time and calculate the redshift $z(r)$ along it, then, initially, z increases from $z = 0$ at the observation event. However, if the ray was emitted at the BB at such a point, where $dt_B/dr \neq 0$, then $z(r)$ will reach a maximum somewhere in the past, and will then decrease, to become $z = -1$ at the intersection of the ray with the BB. The maximum redshift is achieved where $dz/dr = 0$, i.e., from (2.10), where $R_{,tr} = 0$. The hypersurface determined by $R_{,tr} = 0$ is observer-independent; this is the MRH described in Sec. I. From (2.11), using (2.3), we have

$$\begin{aligned} R_{,tr} &= \frac{E_{,r}}{2E} R_{,t} - \frac{M}{R^2} \left(\frac{3E_{,r}}{2E} - \frac{M_{,r}}{M} \right) (t - t_B) \\ &+ \frac{M}{R^2} t_{B,r} \end{aligned} \quad (3.1)$$

when $E \neq 0$, and

$$R_{,tr} = \left(\frac{M_{,r}}{3M} + \frac{\sqrt{2M}}{R^{3/2}} t_{B,r} \right) R_{,t} \quad (3.2)$$

when $E = 0$. From now on, the cases $E > 0$ and $E < 0$ have to be considered separately.

$E > 0$

Using (2.3), (2.4) and (3.1), the equation $R_{,tr} = 0$ is rewritten as

$$(t - t_B) \left[\frac{E_{,r}}{2E} F_1(\eta) + \frac{3}{r} \right] = -t_{B,r}, \quad (3.3)$$

where

$$F_1(\eta) \stackrel{\text{def}}{=} \frac{\sinh \eta (\cosh \eta - 1)}{\sinh \eta - \eta} - 3. \quad (3.4)$$

The conditions for no shell crossings in the case $E > 0$ are [21], [12]

$$E_{,r} > 0, \quad t_{B,r} < 0. \quad (3.5)$$

Hence, in a region with no shell crossings,² the right-hand side of (3.3) is positive, and so is the coefficient of $F_1(\eta)$. We also have

$$F_1(\eta) > 0, \quad dF_1/d\eta > 0 \quad (3.6)$$

for all $\eta > 0$. From this follows

Lemma 3.1

For every $\varepsilon > 0$ there exists a $\delta > 0$ such that $t - t_B < \varepsilon$ if $|t_{B,r}| < \delta$.

The proof is given in Appendix B.

Consequently, by choosing $|t_{B,r}|$ sufficiently small, t can be made arbitrarily close to t_B ; in particular, earlier than the recombination time. Thus, the MRH can be hidden in the pre-recombination epoch, where the zero-pressure L–T models cannot apply, and blueshifts will not arise in the L–T region.

Note that (3.3) – (3.6) imply that the MRH does not exist if $t_{B,r} = 0$ everywhere. (Formally, (3.3) implies then $t = t_B$, but we know from elsewhere [6, 7] that in this case $z \rightarrow \infty$ at the BB, so $dz/dr \rightarrow \infty$, too.) This holds, for example, in the L–T model of Ref. [19].

² It has to be recalled that in the L–T model that reproduces (2.14) with $t_{B,r} \equiv 0$, a region with shell crossings does exist [19, 22]. This is why we cannot assume that the whole model is free of shell crossings; it is to be expected that shell crossings will also exist when $|t_{B,r}|$ is small but nonzero.

$$\underline{E = 0}$$

Then, using (3.2), the equation $R_{,tr} = 0$ implies

$$R = 2^{1/3} M_0 r^{5/3} (-t_{B,r})^{2/3}. \quad (3.7)$$

The no-shell-crossing condition here is $t_{B,r} < 0$. Thus, by choosing $|t_{B,r}|$ sufficiently small, we can make R arbitrarily close to zero, i.e. to the BB. So, again, the blueshifts can be removed from the L-T region.³

$$\underline{E < 0}$$

Using (2.6) and (3.1) and assuming $0 \leq \eta \leq \pi$ (the Universe is expanding), $R_{,tr} = 0$ is rewritten as

$$(t - t_B) \left[\frac{E_{,r}}{2E} G_1(\eta) + \frac{3}{r} \right] = -t_{B,r}, \quad (3.8)$$

where

$$G_1(\eta) \stackrel{\text{def}}{=} \frac{\sin \eta (1 - \cos \eta)}{\eta - \sin \eta} - 3. \quad (3.9)$$

In this case, the analogue of Lemma 3.1 cannot be proved, since the function G_1 is negative and decreasing for all $0 < \eta < \pi$, while the no-shell-crossing conditions do not imply a unique sign for $E_{,r}/E$.⁴ So, this case was considered for completeness only. It is known [19] that with $t_{B,r} \equiv 0$ the relation (2.13) – (2.14) can be duplicated in an L-T model only with $E > 0$ at all $r > 0$. Thus, it is to be expected that the model with $E < 0$ at $r > 0$ will be inapplicable also when $|t_{B,r}|$ is small but nonzero.

IV. THE MAXIMUM-REDSHIFT HYPERSURFACE IN THE L-T(t_B) MODEL

In the L-T(t_B) model, the nonconstant $t_B(r)$ is uniquely (numerically) determined by (2.10), so dt_B/dr is also fixed. Consequently, the method of removing blueshifts from the L-T epoch, presented in Sec. III, cannot be applied here. As will be seen, blueshifts in this model occur later than the recombination epoch in a large region around the center. A radical solution of the problems with blueshifts would be to assume that the L-T(t_B) model applies only as far back in time as $dz/dr > 0$ along radial rays. However, it is useful to know exactly where the blueshift-generating region is located and how the blueshifts would make themselves visible to a late-time observer in this model. These questions will be dealt with in the remaining part of this paper.

³ But the model with $E = 0$ cannot obey (2.14) [4].

⁴ Since $E(0) = 0$ must hold in order to avoid a permanent central singularity [12], and $E(r) < 0$ at $r > 0$ by assumption in this case, the consequence is $E_{,r} < 0$ in a vicinity of $r = 0$, i.e., $E_{,r}/E > 0$ for small r . However, this argument does not hold for large r . The no-shell-crossing conditions require only that $t_{B,r} < 0$ and $2\pi \left(\frac{3}{2} \frac{E_{,r}}{E} - \frac{M_{,r}}{M} \right) - \frac{(-2E)^{3/2}}{M} t_{B,r} < 0$ [12].

As in Sec. III, the location of the MRH in spacetime is determined by the equation $R_{,tr} = 0$. However, caution is required in interpreting the solution. Equation (2.10) shows that $R_{,tr}$ might vanish also at those points, where $z \rightarrow \infty$. See below for more on this.

Using (2.20) for $R_{,r}$, the equation $R_{,tr} = 0$ is

$$\sqrt{\frac{2M_0 r}{R}} - k = -\frac{M_0 r^3 t_{B,r}}{R^2}, \quad (4.1)$$

where (2.3), (2.17) and (2.8) were used to eliminate $R_{,t}$. With $t_{B,r} < 0$ and $k < 0$, (4.1) is solvable and implicitly defines (via $R(t, r)$) the $t(r)$ function along the MRH.

For numerical handling, it is more convenient to square (4.1) and substitute for R from (2.21), obtaining

$$x^4 + x^3 + k^3 \left(\frac{rt_{B,r}}{4M_0} \right)^2 = 0, \quad (4.2)$$

where

$$x \stackrel{\text{def}}{=} \sinh^2(\eta/2). \quad (4.3)$$

Where $r > 0$ and $t_{B,r} < 0$, the solution of (4.2) obeys

$$0 < x < x_{\text{max}} \stackrel{\text{def}}{=} -k \left(\frac{rt_{B,r}}{4M_0} \right)^{2/3}. \quad (4.4)$$

However, (4.2) implies $x = 0$ at those r , where $t_{B,r} = 0$. This means $\eta = 0$, i.e. $R = 0$. This is the BB, where $z \rightarrow \infty$. The conclusion is that the MRH does not exist along those rays that hit the BB where $t_{B,r} = 0$. Also, (4.2) implies $x = 0$ at $r = 0$. The point determined by $x = 0$ ($\implies \eta = 0$) and $r = 0$ is the central point of the BB, where $R = 0$. But (4.2) was obtained from (4.1) by squaring and multiplying by R^4 . Consequently, the solution of (4.1) is not determined at $r = 0$, although the limit $r \rightarrow 0$ of the solution found at $r > 0$ may exist.

Having found (numerically) $x(r)$, and thus also $\eta(r)$ from (4.3), we find $t(r)$ on the MRH from (2.4):

$$t_{\text{MRH}}(r) = t_B(r) + \frac{M_0}{(-k)^{3/2}} \{ \sinh[\eta(r)] - \eta(r) \}. \quad (4.5)$$

Equation (4.2) was derived assuming that the null geodesics, on which $z(r)$ is calculated, are radial. But it makes no reference to the initial point of the geodesic arc. Consequently, the MRH is observer-independent. The maximal *value* of redshift will depend on the initial point, where $z = 0$, but the *location* of the maximum will not: the maximum along a given geodesic will occur always at the same r .

In order to use (4.5), we need to know the function $t_B(r)$. It was numerically calculated in Ref. [4], but only up to $r \approx 1.05584$ (corresponding to $t_B \approx -0.139454$ NTU), which is not sufficient for the present purpose. Consequently, it had to be re-calculated and extended, and the way of extending needs an explanation.

The numerical step was $\Delta r \approx 5 \times 10^{-6}$. Beginning at

$$r \stackrel{\text{def}}{=} r_c = 1.4131983072777050, \quad (4.6)$$

the numerically calculated t_B became constant,

$$t \stackrel{\text{def}}{=} t_{Bc} = -0.13945554689046649 \text{ NTU}, \quad (4.7)$$

and this value was maintained from step $n = 221923$ for the next 1757 steps (the calculation broke down at $r \stackrel{\text{def}}{=} r_f = 1.4219332552803152$, with the Fortran program saying that $t_B = \text{NaN}$ for all $r > r_f$). So, it was assumed that $t_B(r) = t_{Bc}$ at the contact with the PCPO, and the $t_B(r)$ curve was extended “by hand” as the straight line $t = t_{Bc}$. The extended graph of $t_B(r)$ is shown in Fig. 1 together with $t_{\text{MRH}}(r)$. Given the table of values of $t_B(r)$, the $t_{B,r}(r)$ needed to solve (4.2) is easy to calculate.

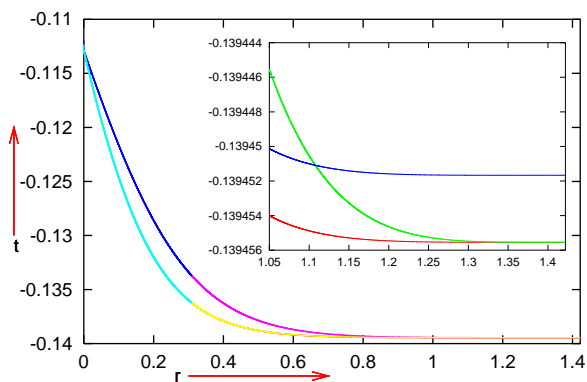


FIG. 1: **Main panel:** The functions $t_B(r)$ (lower curve) and $t_{\text{MRH}}(r)$. The $t_B(r)$ acquires the constant value t_{Bc} given by (4.7) on approaching the right end. **Inset:** Closeup view of the region, where $t_B(r)$ (the lowest curve) and $t_{\text{MRH}}(r)$ (the curve with the uppermost left end) become tangent. The third curve is the $t_{\text{rec}}(r)$ of (4.8). See text for more explanation.

The inset in Fig. 1 includes the graph of the recombination time, given approximately by [23]

$$t_{\text{rec}}(r) - t_B(r) = 3.8 \times 10^5 \text{ y} = 3.88 \times 10^{-6} \text{ NTU}. \quad (4.8)$$

This will be used for illustration only. The correct $t_{\text{rec}}(r)$ would have to be calculated by determining the $t - t_B$, at which the density in our model becomes equal to the density at recombination in the Λ CDM model. However, this more exact calculation would introduce only a small correction to (4.8), which would not substantially improve the usefulness of it. As further calculations will show, along most rays both the MRH and the ZRH will occur much later than the time given by (4.8). At the scale of the main panel of Fig. 1, the graph of $t_{\text{rec}}(r)$ is indistinguishable from the graph of $t_B(r)$.

The following facts about Fig. 1 need to be noted:

1. The right end of the graphs is at $r = 1.422$. This is where $z(r)$ along the PCPO was found to be unmanageably large ($z \approx 1.6237 \times 10^{229}$) [4], signaling the near-contact of the PCPO with the BB.

2. The $t_{\text{rec}}(r)$ and $t_{\text{MRH}}(r)$ curves intersect at $r \stackrel{\text{def}}{=} r_x \approx 1.107817$. For $r > r_x$, the MRH is earlier than the hypersurface of last-scattering, and thus becomes astrophysically irrelevant, as the L-T model is inadequate for describing the epoch $t < t_{\text{rec}}(r)$.

3. The redshift corresponding to r_x is $z_x \approx 57.88$. This is much larger than $z_{\text{far}} = 10$ [24], the largest observed redshift apart from CMB.

V. LIGHT RAYS INTERSECTING THE PAST LIGHT CONE OF THE PRESENT CENTRAL OBSERVER

The profile of the PCPO calculated in Ref. [4] is shown in the main panel of Fig. 2. It becomes tangent to the $t_B(r)$ at $r \approx 1.42182$. We will now determine the intersections with the ZRH for rays received by observers sitting on the PCPO at a few characteristic positions.

A. Ray B

Consider the observer O_b (“b” for “border”) who intersects the PCPO at $z = z_{\text{fSN}} = 1.9$. As noted above, this is the largest observed redshift corresponding to a supernova of type Ia [8]. The functions $z(r)$, $t(r)$ and $R(r)$ along the PCPO were calculated in Ref. [4]. In their tables of values, the z nearest to z_{fSN} and the corresponding r , t and R at the PCPO are

$$z_b = 1.900028454789241, \quad (5.1)$$

$$r_b = 0.3486128555616366, \quad (5.2)$$

$$t_b = -0.10726235253032952, \quad (5.3)$$

$$R_b = 0.0594055585753355889. \quad (5.4)$$

Equations (5.2) and (5.3) define the initial conditions for the outgoing radial light ray that O_b receives at the moment of intersecting the PCPO. It was calculated backward from this event and will be called ray B. It is the increasing curve in Fig. 2.

Figure 3 shows the graph of $z(r)$ along ray B. The numerical calculation broke down near the singularity, so the value of z at $t = t_B$ could not be calculated, but it is known to be -1 there [6, 7]. The nearest value to -1 that was yet calculated was $z = -0.85255346539197885$, achieved at $r = 0.17430456376783951$. The right end of the graph is at the r_b given by (5.2), where the initial value on ray B was $z = 0$.

The maximal redshift along this ray is $z = 0.63536180471132442$, achieved at

$$\begin{pmatrix} r \\ t \end{pmatrix}_{\text{bmax}} = \begin{pmatrix} 0.19233778370400151 \\ -0.12814671882472262 \end{pmatrix}. \quad (5.5)$$

This maximum fits on the $t_{\text{MRH}}(r)$ curve from Fig. 2 up to better than 2×10^{-7} NTU = 19 600 y.

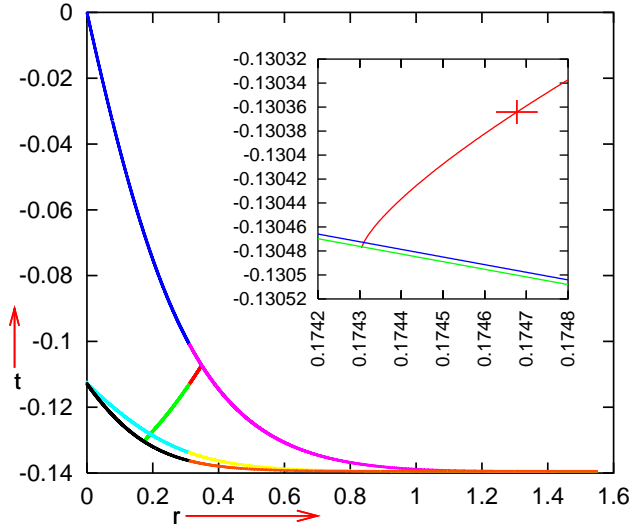


FIG. 2: **Main panel:** The uppermost curve is the profile of the past light cone of the present central observer. The other two decreasing curves are those from the main panel of Fig. 1. The increasing curve is ray B. See text for more explanation. **Inset:** Magnified view of the neighbourhood where $z < 0$ along ray B. The two decreasing lines are $t_B(r)$ (lower) and $t_{\text{rec}}(r)$ of (4.8). The increasing curve is ray B. The cross marks the point where $z = 0$. The t_{MRH} profile is far above the upper margin.

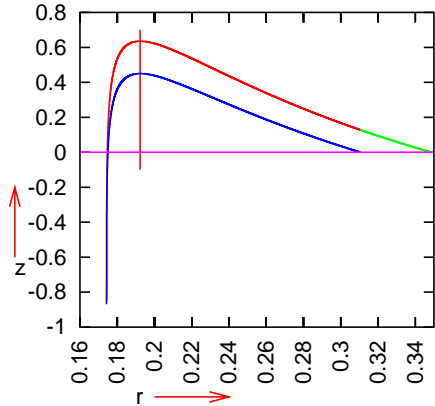


FIG. 3: Redshift $z(r)$ along ray B, calculated from the initial point at the past light cone of the present central observer (upper curve) and from the initial point at the intersection of ray B with $r = r_{\text{AH}}$. The vertical bar marks $r = r_{\text{bmax}}$ given by (5.5). More explanation in the text.

For illustration, Fig. 3 contains also the graph of redshift along ray B, with the initial value $z = 0$ not at the PCPO, but at the intersection of ray B with the line $r = r_{\text{AH}}$. As predicted, the second maximum is at a different z , but at r' , for which $|r' - r_{\text{bmax}}| \approx 3 \times 10^{-6}$.

B. Ray OB

Consider the second observer O_{ob} (for “old border”) intersecting the PCPO at $z_{\text{ob}} = 0.83$, which is the largest

SNIa redshift measured in the twin projects that first reported the accelerated expansion [10]. Again, from the $z(r)$, $t(r)$ and $R(r)$ tables in Ref. [4] we find the z nearest to z_{ob} , and the corresponding r , t and R on the PCPO:

$$z_{\text{ob}} = 0.8300015499642085, \quad (5.6)$$

$$r_{\text{ob}} = 0.19751142662007609, \quad (5.7)$$

$$t_{\text{ob}} = -0.0743328307281575784, \quad (5.8)$$

$$R_{\text{ob}} = 0.0540017311248809709. \quad (5.9)$$

The ray emitted at the BB and received by O_{ob} at the event given by (5.7) – (5.8) will be denoted OB and is shown in Fig. 4, together with the other curves from Fig. 2. Ray OB goes into the past from the PCPO, reaching the center $r = 0$ at $t = -0.11014300011521007$ NTU. It goes to the other side of the center, but its continuation beyond $r = 0$ is drawn in mirror-reflection.

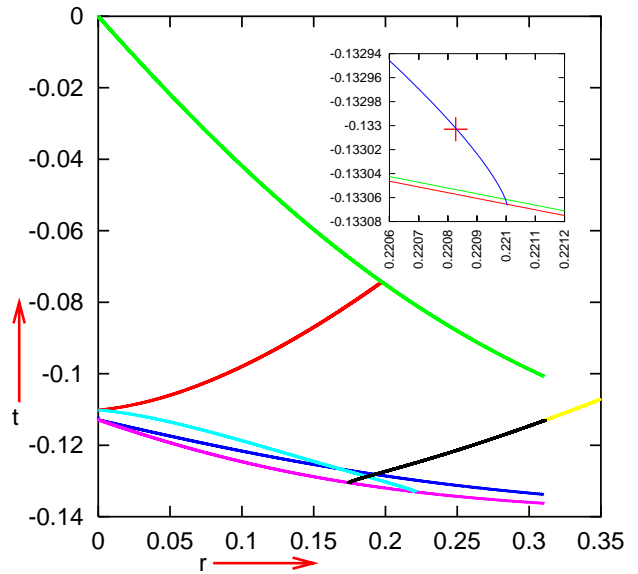


FIG. 4: **Main panel:** The uppermost and the two lowest curves are those from Fig. 2. The two solid arcs at left represent ray OB. The dotted arc at right is ray B. See text for more explanation. **Inset:** Magnified view of the neighbourhood where $z < 0$ along ray OB. The two lowest lines are the same as in the inset in Fig. 2. The third curve is ray OB. The cross marks the point where $z = 0$. The profile of the MRH is again way above the upper margin.

Figure 5 shows the graph of $z(r)$ along ray OB. The graph begins at the r_{ob} given by (5.7), where $z = 0$, and proceeds to the left. The curve $z(r)$ hits the center with $z = 1.2266046302084745$ and goes to the left side of the z -axis, but, as before, the figure shows the mirror-image of the continuation. From this point on, $z(r)$ increases to the maximum $z = 3.0946480957646290$ attained at

$$\begin{pmatrix} r \\ t \end{pmatrix}_{\text{obmax}} = \begin{pmatrix} 0.16821171418720421 \\ -0.12662412927673727 \end{pmatrix}. \quad (5.10)$$

The t_{obmax} given above agrees with the corresponding t on the $t_{\text{MRH}}(r)$ curve to better than 10^{-6} NTU

$= 9.8 \times 10^4$ y. Beyond this maximum, $z(r)$ decreases to $z = -0.85628254978650187$ attained at $r = 0.22100398884102759$.

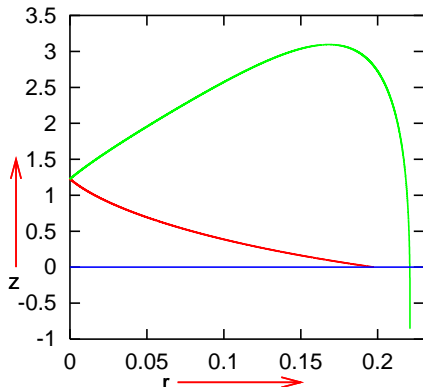


FIG. 5: Redshift $z(r)$ along ray OB.

Note that the redshift in Fig. 5 becomes negative at $r \approx 0.2208$, which is larger than the r_{ob} , given by (5.7). Thus, if our L-T model were matched to a Friedmann background at r between r_{ob} and 0.2208, the ray (followed back in time) would enter the Friedmann region with the redshift still being positive, and would start building up more-positive redshifts from then on. See more on this in Sec. VI.

It is interesting that all the qualitative properties of blueshift described here (blueshift being infinite when $dt_B/dr \neq 0$ at the contact of the ray with the BB, being visible to all observers along the blueshifted ray, perturbing the CMB spectrum) were mentioned without proof by Szekeres already in 1980 [6]; he even drew the MRH profile for $E = 0$ and $t_B(r) = 1/(1+r^2)$.

C. Ray N

The third observer, O_n (for “near”), is placed at such r that the ray she receives at the intersection with the PCPO is emitted from the BB where the function t_B is flat. The placement of O_n was determined by trial and error. Its initial data at the PCPO are

$$z_n = 0.02000194389343255, \quad (5.11)$$

$$r_n = 0.00653692577372784, \quad (5.12)$$

$$t_n = -0.00293913865628162, \quad (5.13)$$

$$R_n = 0.002910104748843882. \quad (5.14)$$

The ray emitted at the BB and received by O_n at the event given by (5.12) – (5.13) will be denoted N and is shown in Fig. 6. Similarly to ray OB, ray N, followed from the initial point given by (5.12) – (5.13) into the past, first reaches the center at $t = -0.00581492733951897989$ NTU, then continues on the

other side of the center, hitting the BB at

$$\begin{pmatrix} r \\ t \end{pmatrix}_{nBB} = \begin{pmatrix} 1.3401983891580524 \\ -0.1394554652960040 \end{pmatrix}. \quad (5.15)$$

At the contact of ray N with the BB, t_B is constant up to better than $\Delta t_B = 10^{-6}$ NTU = 9.8×10^4 y.

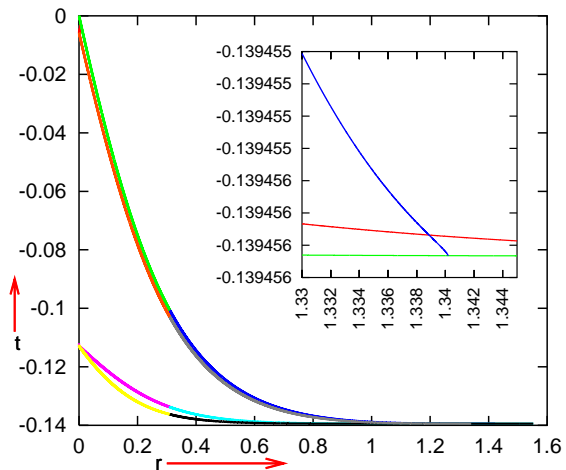


FIG. 6: **Main panel:** The uppermost and the two lowest curves are those from Fig. 2. The arc that nearly coincides with the cone profile is ray N. See text for more explanation. **Inset:** The neighbourhood, where ray N hits the BB. The curves, counted from top to bottom at the left edge, are ray N, $t_{MRH}(r)$ and $t_B(r)$. The recombination time is $\approx 3 \times 10^{-6}$ NTU above the upper edge of the graph. Redshift never becomes negative along ray N, and becomes very large near the BB, see Fig. 7. More explanation in the text.

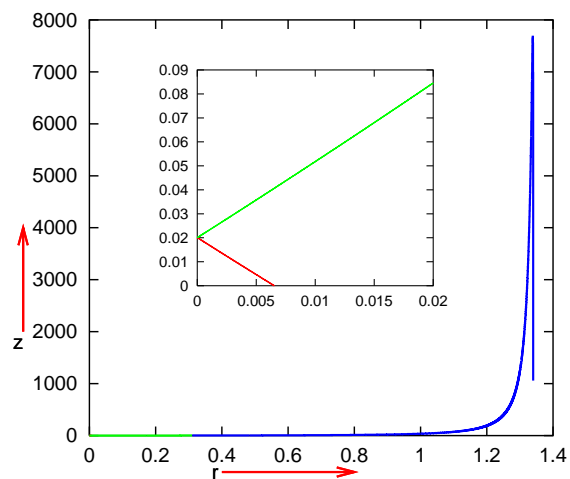


FIG. 7: **Main panel:** Redshift $z(r)$ along ray N from Fig. 6. **Inset:** Closeup view of the left end of the main graph. See explanation in the text.

The redshift along ray N is shown in Fig. 7. The only point along ray N where $z = 0$ is the initial point at the PCPO. Following ray N to the past, z attains the value

0.0200723615789212863 at $r = 0$, then increases up to the maximum $z \approx 7676.412$, attained at

$$\begin{pmatrix} r \\ t \end{pmatrix}_{\text{nmax}} = \begin{pmatrix} 1.3388618129278465 \\ -0.13945554652960040 \end{pmatrix}. \quad (5.16)$$

Then a numerical instability causes z to go down at larger r . This is because, at the level of precision assumed here, where ray N hits the BB, the t_B is “not constant enough” for z to go to infinity. Were O_n placed nearer to the center, ray N would be indistinguishable from the PCPO.

The transition from rays emitted at nonconstant t_B to those emitted at constant t_B is discontinuous. Beginning with the situation shown in Fig. 5 and moving the observer ever closer to the center, the redshift profile changes as follows: the initial point where $z = 0$ moves closer to the $r = 0$ axis, the point of crossing the $r = 0$ line moves down, the maximum of $z(r)$ moves up and to the right, and the final segment of $z(r)$ that goes down becomes ever steeper, approaching vertical. If the observer is close enough to the center, so that the ray (followed back in time) hits the BB where t_B is exactly constant, $z(r)$ goes to infinity at the contact with the BB, and the final steep segment of the curve disappears. Figure 8 shows a graph of $z(r)$ intermediate between the situations in Figs. 5 and 7.

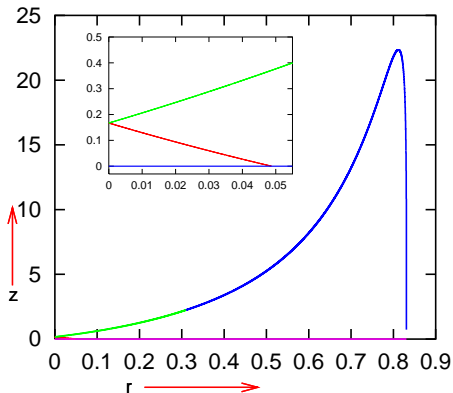


FIG. 8: Redshift $z(r)$ along a ray received by an observer placed between O_{ob} and O_n . See explanation in the text. The inset shows $z(r)$ near $r = 0$.

VI. THE L-T(t_B) MODEL MATCHED TO FRIEDMANN

Now we come back to the remark made in the paragraph after (5.10). The necessary and sufficient condition for matching an L-T to a Friedmann model [12] is that at the boundary hypersurface the functions $M(r)$, $E(r)$ and $t_B(r)$ go over in a continuous (not necessarily differentiable) way into their Friedmann counterparts. Our functions $M(r)$ and $E(r)$ have Friedmannian forms from the beginning. So, it is enough to assume that $t_B(r)$ be-

comes constant at the boundary value of r .⁵ As stated in the aforementioned remark, the r at the boundary should be between the r_{ob} given by (5.7) and $r = 0.2208$. So we choose the intermediate value r_F , where

$$\begin{pmatrix} r \\ t_B \end{pmatrix}_F = \begin{pmatrix} 0.2100014577175866 \\ -0.1325224690059549 \end{pmatrix}. \quad (6.1)$$

The time on the PCPO at this boundary is

$$t_F = -0.0778299400591163509 \text{ NTU}. \quad (6.2)$$

From the tables of values of $t(r)$ and $z(r)$ along ray OB we find that at the r_F given above we have

$$\begin{pmatrix} t \\ z \end{pmatrix}_{\text{OB } F} = \begin{pmatrix} -0.13144220116062100 \\ 2.2425612667236408 \end{pmatrix}. \quad (6.3)$$

Ray OB is now continued through $r = r_F$ into the Friedmann region, with the above as the initial data for it.

In the Friedmann region, (2.9) simplifies to

$$\frac{dt}{dr} = \pm \frac{S(t)}{\sqrt{1 - kr^2}}, \quad (6.4)$$

where $S(t) \stackrel{\text{def}}{=} R/r$. Using (2.4), (2.8) and (2.17), this can be integrated with the result

$$\eta(r) + C = \pm \ln \left(\sqrt{-kr} + \sqrt{1 - kr^2} \right), \quad (6.5)$$

where $\eta(r)$ is the same as in (2.4) and C can be found from the initial condition

$$\eta_F + C = \pm \left[\ln \left(\sqrt{-kr} + \sqrt{1 - kr^2} \right) \right]_F, \quad (6.6)$$

with r_F given by (6.1), and η_F calculated from (2.4):

$$\sinh \eta_F - \eta_F = \frac{(-k)^{3/2}}{M_0} (t_F - t_{BF}). \quad (6.7)$$

The t_F and t_{BF} are given by (6.1) and (6.3).

So, the construction of the Friedmann light cone and the calculation of redshift along it goes as follows. The consecutive values of r are taken from the same table as in the previous calculations. Given the value of r , the $\eta(r)$ is calculated from (6.5) using (6.6) for C , then $t(r)$ and $S(t(r))$ along the light cone are calculated from (2.4) using (2.8), (2.17) and (6.1). Finally, with $S(t(r))$ known, the redshift along the light cone is calculated from [12]

$$1 + z(r) = z_F + S_F/S(t(r)). \quad (6.8)$$

Figure 9 shows the continuation of $t_B(r)$ (the lowest line) and of ray OB through the boundary of the L-T and

⁵ The model we consider already coincides with Friedmann for $r > r_c$, where r_c is given by (4.6). But to make the intended point, we need to match it to Friedmann at r_F given by (6.1).

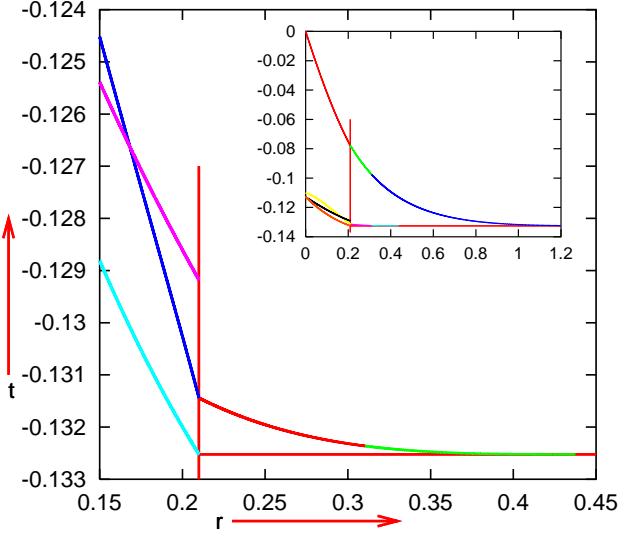


FIG. 9: **Main panel:** Continuation of $t_B(r)$ (the lowest line) and of ray OB into the Friedmann region. The vertical line marks the L-T/Friedmann boundary at $r = r_F$ given by (6.1). The descending line that ends at the boundary is the profile of the MRH. **Inset:** The contents of the main panel shown together with the complete past light cone of the present central observer extended into the Friedmann region.

Friedmann regions.⁶ The line that ends at the boundary is the MRH; it does not exist in the Friedmann region because there the maximal redshift is infinite.

Figure 10 shows the continuation of $z(r)$ from Fig. 5 through the boundary of the L-T and Friedmann regions. The function $z(r)$ was decreasing in the L-T region close to its boundary, but becomes increasing in the Friedmann region, and increases until it becomes too large to handle by the Fortran program. This happens at

$$\begin{pmatrix} r \\ z \end{pmatrix}_{\text{large}} = \begin{pmatrix} 0.43753244000885227 \\ 11861354545.253244 \end{pmatrix}. \quad (6.9)$$

This is, not accidentally, the same r_{large} at which the continuation of ray OB into the Friedmann region becomes tangent to the constant- t_B line.

The matching of the L-T and Friedmann models does not solve the problem of blueshifts. The PCPO continued into the Friedmann region would still encounter blueshifted rays emitted in the L-T(t_B) region. Figure 11 shows one such exemplary ray. It was calculated in two stages:

1. Equations (6.5) – (6.8) (with the + sign in (6.5) – (6.6)) were used to calculate $t(r)$ and $z(r)$ back in time

⁶ Ray OB, $t_B(r)$ and $z(r)$ can be made differentiable at $r = r_F$ by inserting an interpolating arc between the $t_B(r)$ of the L-T region and the constant t_B of the Friedmann region. The general matching conditions do not require this [12].

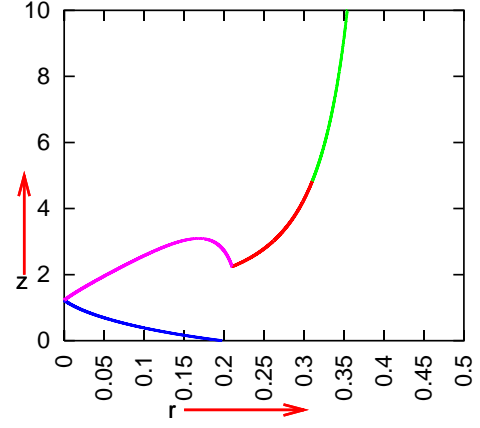


FIG. 10: Continuation of $z(r)$ from Fig. 5 into the Friedmann region. The redshift becomes too large to handle at $r = r_{\text{large}}$ given by (6.9).

from the initial point at the PCPO, with the coordinates

$$\begin{pmatrix} r \\ t \end{pmatrix}_{\text{ei}} = \begin{pmatrix} 0.3000029697185931 \\ -0.0958721393954025947 \end{pmatrix}. \quad (6.10)$$

The ray reached the L-T/Friedmann boundary at

$$\begin{pmatrix} r \\ t \end{pmatrix}_{\text{eF}} = \begin{pmatrix} 0.2100014577175866 \\ -0.10919095912654034 \end{pmatrix} \quad (6.11)$$

with the redshift

$$z_{\text{eF}} = 0.37819933974218056. \quad (6.12)$$

2. Using (6.11) – (6.12) as initial data, (2.9) – (2.10) (again with the + sign) were integrated to determine the continuation of $t(r)$ and $z(r)$ into the L-T region. The proximity of the singularity did not allow $t(r)$ to end up with a vertical tangent, and the $t(r)$ curve actually overshoot the BB (as can be seen on close inspection of the inset in Fig. 11). Its end point is at

$$\begin{pmatrix} r \\ t \end{pmatrix}_{\text{ee}} = \begin{pmatrix} 0.0997339231053535613 \\ -0.12458819154593222 \end{pmatrix} \quad (6.13)$$

with the last z yet calculated being

$$z_{\text{ee}} = -0.8051202078031556. \quad (6.14)$$

In addition to this ray, the main panel in Fig. 11 shows the PCPO (the uppermost curve) and $t_B(r)$ (the lowest curve), both continued into the Friedmann region. The third decreasing line is the MRH profile, and the vertical line marks the L-T/Friedmann boundary.

The inset in Fig. 11 shows the final segment of the boundary-crossing ray, on which $z(r)$ becomes negative. The coordinates of the point, at which $z = 0$ are

$$\begin{pmatrix} r \\ t \end{pmatrix}_{\text{ez0}} = \begin{pmatrix} 0.099836402226740395 \\ -0.12454907240930377 \end{pmatrix}. \quad (6.15)$$

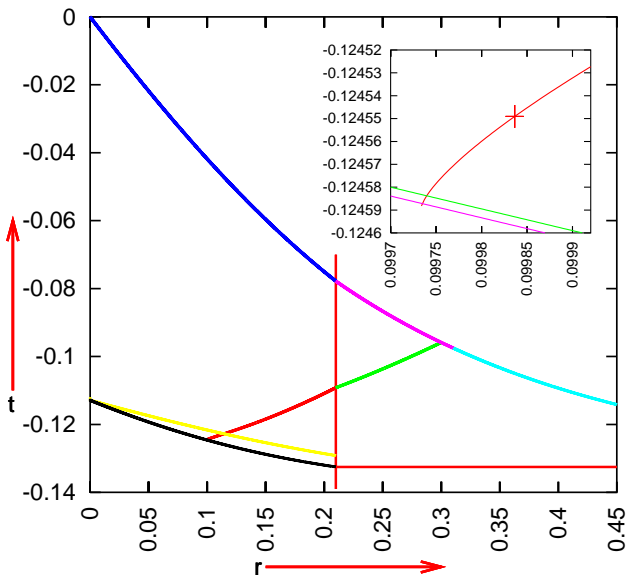


FIG. 11: **Main panel:** The L–T(t_B) model matched to Friedmann across $r = r_F$, and the ray crossing the boundary that displays blueshift in the Friedmann region. See text for more explanation. **Inset:** The boundary-crossing ray in the neighbourhood of the Big Bang. The decreasing lines are $t_B(r)$ (lower) and $t_{\text{rec}}(r)$ given by (4.8) (upper). The cross marks the point on the ray where $z = 0$. The maximum-redshift hypersurface is far above the upper margin.

The profile of $z(r)$ along this ray is shown in Fig. 12. The coordinates of the maximum in z are

$$\begin{pmatrix} r \\ t \end{pmatrix}_{\text{emax}} = \begin{pmatrix} 0.11435427775654181 \\ -0.12276948639632553 \end{pmatrix} \quad (6.16)$$

and the maximal value of z is

$$z_{\text{emax}} = 0.88302700024316949. \quad (6.17)$$

The point given by (6.16) lies on the MRH profile up to better than $\Delta t = 3.6 \times 10^{-8}$ NTU = 3528 y (the r coordinates agree by construction).

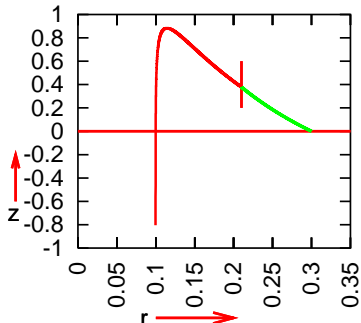


FIG. 12: The redshift along the boundary-crossing ray from Fig. 11. The vertical bar marks $r = r_F$ given by (6.1).

Comparing such a composite model with observations might be difficult. As seen from Fig. 10, the redshift

along ray OB increases with r only up to a maximum attained at r_{obmax} given by (5.10), then decreases with increasing r up to the L–T/Friedmann boundary, and then starts to increase again. In astronomy, it is assumed that redshift is a monotonically increasing function of distance (and of look-back time); in fact, redshift is routinely used as a measure of distance to objects far from the observer. To test this model, a method of determining distance independent of redshift would have to be introduced.

VII. CONCLUSIONS

In a general L–T model with nonconstant $t_B(r)$, choosing t_B nearly constant (i.e., with a sufficiently small $|dt_B/dr|$), one can move the maximum-redshift hypersurface (MRH) to times earlier than recombination. At those times, the zero-pressure L–T model cannot describe the Universe. Consequently, no blueshifts will be observed in the after-recombination epoch (Sec. III).

The rest of the paper is devoted to investigating blueshifts in one particular L–T model, called L–T(t_B). It is the one derived in Ref. [4], in which the Λ CDM function $D_L(z)$ is duplicated using nonconstant t_B alone; the $E(r) = -kr^2/2$ with k given by (2.18) is the same as in a Friedmann model. In Sec. IV, the MRH is determined for this model. In Sec. V, the redshift/blueshift profiles along three characteristic rays in this model are calculated and displayed. In Sec. VI, the L–T(t_B) model matched to Friedmann is investigated. The matching hypersurface is chosen so that the L–T(t_B) region encompasses all the type Ia supernovae of the original project [9, 10]. This matching does not solve the problem of blueshifts because observers in the Friedmann region would receive blueshifted rays emitted from the nonconstant Big Bang in the L–T(t_B) region.

The final verdict on the L–T(t_B) model is thus: if we insist on applying it all the way back to the recombination time, then blueshifted rays will inevitably cross the past light cone of the present central observer at sufficiently large z . In the example shown in Fig. 11, blueshifts would be present beyond $z \approx 1.50087$. But this argument does not “rule out” general L–T models with nonconstant t_B , as shown in Sec. III.

To the attempts at discrediting the usefulness of the L–T model (or more general ones) for cosmology, one can give a philosophical answer: objects existing in Nature do not fulfil mathematical assumptions with perfect precision. Assumptions such as spherical symmetry, axial symmetry, isolated body, free fall, ideal gas, incompressible fluid, are in reality fulfilled only up to some degree of approximation. Why should the Universe be an exception and arise in an exactly simultaneous Big Bang, when the theory allows the BB to be extended in (comoving)

time?⁷ Anticipating more general solutions of Einstein’s equations, one should even expect the most general BB time to be a function of all three spatial variables, possibly limited in generality by the constraint equations.

We generally agree that the Nature acts through mathematics. If so, then it is reasonable to assume that it takes the tools from a generic set, e.g., not a constant function when nonconstant ones are admissible, not a function of 2 variables when 3 are possible, etc. Would Nature ignore all this freedom in order to keep the inflation hypothesis still alive and mainstream astronomers feeling safe with their current knowledge?

Appendix A: Remarks about Ref. [1]

A comment on the terminology must be made here. The accelerated expansion of the Universe is not an observed phenomenon. What is observed are redshifts and apparent brightnesses of the SNIa. In the papers that first reported accelerated expansion [9, 10], these observations were interpreted using exclusively the Friedmann models. Within this class of models, the best fit between the model parameters and the observations is achieved when the curvature index k is zero, and the cosmological constant Λ has a value that is responsible for approx. 70% of the present energy-density of the Universe (the current figure is 68% [16]). The accelerated expansion, driven by Λ , is thus a model-dependent element of interpretation of observations.

The earliest attempt at re-interpreting these observations using a less simplistic model introduced a void around the center of symmetry [25–27] (a lower-density Friedmann region surrounded by a higher-density Friedmann background). This pioneering experiment caused that the term “void models of acceleration” is now just reflexively used by many authors to denote attempts at explaining the SNIa observations using models with inhomogeneous matter distribution. This term is misleading and, in fact, incorrect: several such models contain condensations instead of voids around the center; see, for example, Refs. [28] and [19].

The critical remarks presented below concern the concrete L–T model chosen by the author as a basis for his considerations, but not the technical details of Ref. [1].

1. The author of Ref. [1] chose for his investigation the L–T model with

$$E = 0 \quad \text{and} \quad t_B(r) = ae^{-(r/L)^2}, \quad (\text{A1})$$

where a and L are constants. The choice $E = 0$, justified by the desire to consider only the “decaying mode” of perturbation of homogeneity, was too special – see points 2 and 4 below. The choice of $t_B(r)$ was not justified;

it was “convenient”. Then, the author proved that the model defined by (A1) does not pass the observational test of spectral distortions of the light reaching the central observer, and used this as a basis for a far more general claim that “models with significant decaying mode contribution today can be ruled out on the basis of the expected cosmic microwave background spectral distortion”. This leap from the failure of one handpicked example containing two arbitrary constants to the dismissal of the whole class labelled by two arbitrary functions of r is a logical error. By the same logic, one could “rule out” the Robertson – Walker models because one of them (the Einstein Universe) is static, and so “inconsistent with various observations”. What Ref. [1] proved was only the fact that (A1) is not an acceptable choice.

2. To consider the L–T model with a “pure decaying mode” in connection with “void models of acceleration”, the function $t_B(r)$ must duplicate the $D_L(z)$ of (2.14) or another function fitted to the SNIa observations. Thus, it cannot be freely chosen. In Ref. [4] it was proven that, assuming $E/M^{2/3} = -k$ constant (see point 4 below for justification), the function $D_L(z)$ is duplicated only when $t_B(r)$ has a unique shape different from (A1), while $k = -4.7410812$. Consequently, the model (A1) is unrelated to the “void models of acceleration”.

3. The “decaying mode” was chosen for a kill because the author was convinced that the “pure growing mode” had been ruled out already before. Isolating the growing and decaying modes for separate investigations is not productive – see the remarks in Ref. [4]. As shown in Sec. III here, a combination of the two modes allows us to avoid the problem with blueshifts completely.⁸ The vocabulary of growing and decaying modes is borrowed from investigations in linearized Einstein equations and is not useful in the exact theory. Within the exact theory, it is more instructive to deal with quantities that have direct physical meaning, for example, with density or velocity distributions at different hypersurfaces of constant time [18, 29, 30].

4. Even so, the “pure decaying mode” is not correctly defined in Ref. [1]. The increasing perturbations of homogeneity are not generated by “small-amplitude variations in spatial curvature”, but by variations, not necessarily small, in the function $E/M^{2/3}$. Thus, to isolate a pure decaying mode, one must assume $E/M^{2/3} = \text{constant}$, as was done in Refs. [4, 5, 31] and [32], and not $E = 0$, as did the author of Ref. [1].

5. With $t_B(r)$ given by (A1), the function dt_B/dr is nonzero for all r (unlike in Ref. [4] and in the present paper, where dt_B/dr becomes exactly zero at a finite r). Therefore, even the primary CMB ray, along which spectral distortions are calculated in Ref. [1], will reach

⁷ By the way, why should it be exactly homogeneous in the large and exactly spatially flat in addition?

⁸ As proved in Ref. [4], when $E = 0$, the $D_L(z)$ relation of the Λ CDM model cannot be reproduced. This case was included in Sec. III for completeness only.

the present central observer with a blueshift, unless the values of a and L are suitably chosen. The intersection of this ray with the ZRH can be pushed to before the recombination epoch by choosing L sufficiently small, but Ref. [1] does not say whether this was actually taken care of. Without this, one considers blueshifts being distorted by blueshifts.

Appendix B: The proof of Lemma 3.1

Let $-t_{B,r} = \varepsilon > 0$ at a given r (from (3.5)). We shall prove that $t \rightarrow t_B$ when $\varepsilon \rightarrow 0$.

In constructing the proof it must be remembered that, given $t_B(r)$, the function $E(r)$ is determined by (2.13) – (2.14). Consequently, when $|t_{B,r}|$ is decreased at a given r , we have to take into account that $E_{,r}/(2E)$ in (3.3) will thereby also change, and we do not know how.

Going from $-t_{B,r} = \varepsilon > 0$ to a lower value $-t_{B,r} = \varepsilon_2 > 0$ causes the product on the left-hand side of (3.3)

to also decrease. If it is $(t - t_B)$ that decreases, then the thesis is proved. If it is the other factor that decreases, then, in a region with no shell crossings, it may not become smaller than $3/r$. This is because $F_1(\eta) > 0$ (from (3.6)), $E > 0$ (by assumption in this case) and $E_{,r} > 0$ (when there are no shell crossings), while $3/r$ is independent of $t_{B,r}$: the value of r only depends on the point at which the whole analysis is done. Since we can make $(-t_{B,r})$ arbitrarily small, and $\left[\frac{E_{,r}}{2E} F_1(\eta) + \frac{3}{r}\right]$ has the lower bound $3/r$, decreasing $(-t_{B,r})$ will eventually cause $(t - t_B)$ to decrease, too. \square

This proof fails when shell crossings are present ($E_{,r} < 0$) – see the footnote in the paragraph below (3.5).

Acknowledgements: I am grateful to Michał Szurek for his help in formulating the concluding paragraph, and to Jim Zibin for a discussion that helped to clarify a few points.

-
- [1] J. P. Zibin, *Phys. Rev.* **D84**, 123508 (2011).
- [2] G. Lemaître, *Ann. Soc. Sci. Bruxelles* **A53**, 51 (1933); English translation as a Golden Oldie in *Gen. Relativ. Gravit.* **29**, 637 (1997).
- [3] R. C. Tolman, *Proc. Nat. Acad. Sci. USA* **20**, 169 (1934); reprinted as a Golden Oldie in *Gen. Relativ. Gravit.* **29**, 931 (1997).
- [4] A. Krasinski, *Phys. Rev.* **D89**, 023520 (2014) + erratum *Phys. Rev.* **D89**, 089901(E) (2014).
- [5] H. Iguchi, T. Nakamura and K. Nakao, *Progr. Theor. Phys.* **108**, 809 (2002).
- [6] P. Szekeres, in: *Gravitational Radiation, Collapsed Objects and Exact Solutions*. Edited by C. Edwards. Springer (Lecture Notes in Physics, vol. 124), New York, pp. 477 – 487 (1980).
- [7] C. Hellaby and K. Lake, *Astrophys. J.* **282**, 1 (1984) + erratum *Astrophys. J.* **294**, 702 (1985).
- [8] D. O. Jones *et al.*, *Astrophys. J.* **768**, 166 (2013).
- [9] A. G. Riess *et al.*, *Astron. J.* **116**, 1009 (1998).
- [10] S. Perlmutter *et al.*, *Astrophys. J.* **517**, 565 (1999).
- [11] A. Krasinski, *Inhomogeneous Cosmological Models*, Cambridge University Press 1997, 317 pp, ISBN 0 521 48180 5.
- [12] J. Plebański and A. Krasinski, *An Introduction to General Relativity and Cosmology*. Cambridge University Press 2006, 534 pp, ISBN 0-521-85623-X.
- [13] H. Bondi, *Mon. Not. Roy. Astr. Soc.* **107**, 410 (1947); reprinted as a Golden Oldie in *Gen. Relativ. Gravit.* **31**, 1777 (1999).
- [14] M.-N. Célérier, *Astronomy and Astrophysics* **353**, 63 (2000).
- [15] K. Bolejko, A. Krasinski, C. Hellaby and M.-N. Célérier, *Structures in the Universe by exact methods – formation, evolution, interactions*. Cambridge University Press 2010, 242 pp, ISBN 978-0-521-76914-3.
- [16] Planck collaboration, *Planck* 2013 results. XVI. Cosmological parameters. arXiv 1303.5076; to be published in *Astronomy and Astrophysics*.
- [17] C. Quercellini, L. Amendola, A. Balbi, P. Cabella, M. Quartin, *Phys. Reports* **521**, 95 – 134 (2012).
- [18] A. Krasinski and C. Hellaby, *Phys. Rev.* **D69**, 043502 (2004).
- [19] A. Krasinski, *Phys. Rev.* **D90**, 023524 (2014).
- [20] <http://www.asknumbers.com/LengthConversion.aspx>
- [21] C. Hellaby and K. Lake, *Astrophys. J.* **290**, 381 (1985) + erratum *Astrophys. J.* **300**, 461 (1986).
- [22] A. Krasinski, *Phys. Rev.* **D90**, 064021 (2014).
- [23] <http://astronomy.swin.edu.au/cosmos/e/epoch+of+recombination>
- [24] R. McMahon, Quasars and Galaxies at the Highest Redshifts. Crafoord Symposium 2005, http://powershow.com/view/24faaf-OTQ2Y/Quasars_and_Galaxies_at_the_Highest_Redshifts_powerpoint_ppt_presentation
- [25] K. Tomita, *Astrophys. J.* **529**, 38 (2000).
- [26] K. Tomita, *Mon. Not. R. Astron. Soc.* **326**, 287 (2001).
- [27] K. Tomita, *Progr. Theor. Phys.* **106**, 929 (2001).
- [28] M.-N. Célérier, K. Bolejko and A. Krasinski, *Astronomy and Astrophysics* **518**, A21 (2010).
- [29] A. Krasinski and C. Hellaby, *Phys. Rev.* **D69**, 023502 (2004).
- [30] K. Bolejko, A. Krasinski and C. Hellaby, *Mon. Not. Roy. Astr. Soc.* **362**, 213 (2005).
- [31] C.-M. Yoo, T. Kai and K. Nakao, *Progr. Theor. Phys.* **120**, 937 (2008).
- [32] C.-M. Yoo, *Progr. Theor. Phys.* **124**, 645 (2010).